Investigation on dung beetle's (Heliocopris Hope, 1838) chitosan valorisation for hydrogel 3D printing

Xiaomin Yu Godeau, Freddy Jocelyne Andrianandrasana, Olga Volkova, Caroline R Szczepanski, Arnaud Zenerino, Olivier Montreuil, René-Paul Godeau, Pavel Kuzhir, Guilhem Godeau

Investigation on dung beetle's (*Heliocopris* Hope, 1838) chitosan valorisation for hydrogel 3D printing.

Xiaomin Yu Godeau[1], Freddy Jocelyne Andrianandrasana[1,2], Olga Volkova[2], Caroline R. Szczepanski[3], Arnaud Zenerino[1], Olivier Montreuil[4], René-Paul Godeau[1,2], Pavel Kuzhir[2], Guilhem Godeau[1,2]*

[1] *Université Côte d'Azur, IMREDD, 06200 Nice, France*

[2] *Université Côte d'Azur, CNRS UMR 7010 INPHYNI, Parc Valrose Nice, 06108 France*

[3] *Department of Chemical Engineering and Materials Science, Michigan State University, East Lansing, MI 48824 USA*

[4] *UMR 7179 MNHN/CNRS, MECADEV, Muséum National d'Histoire Naturelle, Entomologie, CP 50, 45 rue Buffon, 75231 Paris cedex 05, France*

Tel: (+33) 4 89 15 29 04

E-mail: guilhem.godeau@univ-cotedazur.fr

Abstract

Biopolymers and their derivatives are materials with increasing interest for industry and especially for sustainable engineering development. Among such kind of materials, carbohydrate polymer like highly deacetylated chitin (chitosan) is widely used for a wide range of applications, including material and biomedical developments. The majority of industrially produced chitosan is based on chitin extracted from crustacean exoskeleton. However, with increase of interest on this material, chitosan's production will rapidly become insufficient and other species should be investigated as new sources of chitosan. In the present work, we focus on the preparation of chitosan from giant dung beetles (Genus *Heliocopris*, Hope, 1838). This genus was chosen to show the possibility to take animals that develop and leave near dejection and valuate them for material applications. This work includes all the chitosan extraction procedures, chitosan characterisation IR, SEM, NMR, ash content, and deacetylation degree. Finally, the prepared carbohydrate polymer is used to form hydrogel.

The prepared gel has been characterised and used for 3D printing, to show the compatibility of extracted chitosan with biomaterial application.

Keywords: Dung beetle; biopolymer extraction; chitin; chitosan; hydrogel formation.

1. Introduction

Chitin is one of the most abundant biopolymers in nature, second only to cellulose. It is a linear polymer of β-1,4 linked N-acetylglucosamine [1,2], and is present in numerous animals including arthropods, molluscs, echinoderms and even in mushrooms.[3–7] Due to its macromolecular organisation and strong intramolecular interactions, chitin is very stable and has low solubility in water and most organic solvents. This low solubility makes chitin difficult to use in industrial applications. To increase the solubility of chitin, it is often deacetylated or partially deacetylated, yielding chitosan. More specifically, chitosan corresponds to chitin with a deacetylation degree (DD) greater than 50 %. During deacetylation, amino groups are released along the polymer chain which imparts a higher solubility to chitosan, particularly in slightly acidic water, which makes it more amenable for industrial use. Due to this improved solubility in water, as well as general biocompatibility and biodegradability, chitosan has found use in many application fields including food, medicine, and textiles.[8–13] In medicine, hydrogel formation using chitosan has garnered significant interest. Chitosan-based hydrogels are used in tissue engineering, as injectable materials, for wound healing and also for implants.[10,14–21]

Presently, the most significant source of industrial chitosan is deacetylated chitin extracted from seafood waste, specifically crustacean exoskeletons (e.g., shrimp, crab, lobster or crayfish).[22–27] Given that applications and uses of chitosan are growing, the demand for chitosan is expected to increase significantly in the short-term future. It is therefore necessary to develop alternative sources of chitosan to meet this demand. As mentioned, a wide variety of animals are naturally rich in chitin. While crustaceans have been commonly sourced,

insects may serve as a future source of chitin and chitosan. Furthermore, if insects continue to be considered a potential source of protein for humans, it is interesting to consider potential uses of their waste.[28] Many examples of chitin extraction and chitosan preparation from insects are found in the research literature and a wide diversity of insects have been investigated including locust, cicada, silk-worm, butterfly or beetles.[29–36]

Since 2017, we have studied beetles both as a source of bioinspiration for surface design and more importantly as a potential source of materials such as chitin and chitosan.[37–39] Our interests lie in the possibility of valorising chitosan from beetles. Our first work in this area investigated the potential of large beetles (specifically, *Megasorhina torquata* Drury, 1782 and *Goliathus orientalis* Moser, 1909) as a source of chitosan.[40,41] To diversify our range of studied specimens, we then extended our research field from giant beetles (*Cetoninae*) to other beetles, including *Scarabaeinae* subfamily and more precisely on the dung beetle from genus *Heliocopris* Hope, 1838. While dung beetle breeding conditions may be considered a severe drawback for industrial production, the motivation here is to take animals that develop and live near dejection and convert them into a material appropriate for biomedical applications. Here we investigate the utility of materials extracted from dung beetles in 3D printing, as this is a key first step to for bioprinting.[42–45]

In the present work, we focus on specimens of the genus *Heliocopris* from Republic of Chad (Figure 1), belonging to the species *H. dilloni* Guérin-Méneville, 1849 and investigate the preparation of chitosan from these animals.[46] We characterise the prepared chitosan, and also prepare a mixture of the obtained chitosan and gelatin to develop hydrogels. The rheological properties of the prepared hydrogel are briefly investigated, and we also demonstrate that the prepared hydrogel is suitable for 3D printing and as consequence bioprinting.

Heliocopris sp. from republic of Chad

Figure 1. Examples of *Heliocopris sp.* specimens.

2. Materials and methods

2.1. Materials

All chemicals and solvents were purchased from Aldrich or Merck at synthetic grade and used without further purification. The specimens used in this work come from O. Montreuil collections. They were collected in the Republic of Chad. Observations were made on 6 specimens. All observations were performed on dried specimens.

2.2. Chitin extraction and deacetylation (Chitosan preparation)

Demineralization: Dry *Heliocopris sp.* (10.4 g) was hydrated in a 1M aqueous HCl solution. The solution was then warmed for 2 hours (95 °C). The liquid phase was removed, and the resulting exoskeleton was rinsed with water until reaching a neutral pH. The exoskeleton was then used for deproteination without any further purification nor drying.

Deproteination: After the demineralization protocol (above), the exoskeleton was placed in a 2 M NaOH aqueous solution. The solution was warmed to 95 °C and maintained at this temperature for a period of 36 hours. During this treatment, the solution rapidly turned black. Therefore, the NaOH solution was refreshed hourly during the first 6 hours of the treatment. After the 36 hour period, the liquid phase was removed, and the exoskeleton was rinsed with

fresh water until achieving a neutral pH and directly used in the next step without further purification nor drying.

Bleaching: After deproteination, the exoskeleton was bleached using an aqueous H_2O_2 (50 wt %) solution at room temperature for 4 hours. The bleached exoskeleton was then washed with water and acetone and finally dried in an oven (60 °C), yielding chitin.

Deacetylation: The dry chitin was rehydrated in an aqueous NaOH solution (50 %, w/w). The solution was then warmed (95 °C) overnight. The liquid phase was removed and the solid was washed with fresh water until reaching a neutral pH. The deacetylated chitin (chitosan) was then washed with acetone and dried in an oven at 60 °C. The deacetylation yields 2.3 g of chitosan (Overall yield: 22,1 %).

2.4. Chitosan characterisation

All surface characterizations were performed on *Heliocopris* specimens treated surfaces. All observations were performed in triplicate to obtain standard deviations.

Scanning Electron Microscopy

SEM (scanning electron microscopy) observations were carried out using Phenom Pro X Desktop SEM from Thermo Fisher Scientific. For analysis, dry samples were placed on the SEM support using carbon tape. The samples were then coated with gold using Quorum Q150R S Sputter Coater. The coated samples were then observed in full BSD mode at an accelerating voltage of 5 and 10 kV.

H^1 NMR Characterization

H^1 NMR (nuclear magnetic resonance) were performed on a Brucker 400 MHz, using CF_3COOD as solvent. The NMR chemical shifts are reported in ppm. Due to the polymer structure of chitosan, all reported signals are broad signals.

Chitosan from Heliocopris dilloni: δ_H (400 MHz, CF_3COOD, ppm): 2.84 (H-Ac); 4.06 (H2-Deacetylated); 4.15 - 4.95 (H2 to H6); 5.35 - 5.65 (H1-Acetylated); 5.70 - 5.90 (H1-Deacetylated).

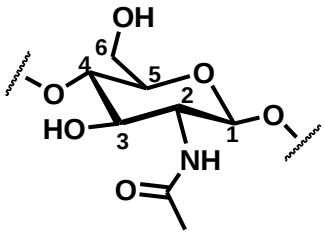

Acetylated unit

Deacetylation degree titration [47]

Dried chitosan (0.1 g) was dissolved in 30 mL of 0.1 M HCl solution. Once the chitosan was completely dissolved, the solution was titrated with a 0.1 M NaOH solution. The pH value was monitored using a pH-meter (pH 110 M from VWR).

FT-IR Characterization

Fourier Transform Infrared spectroscopy (FT-IR) measurements were carried out using a Spectrum Two FT-IR spectrometer from Perkin Elmer with universal ATR accessory. The measurements were performed between 4000 cm^{-1} and 500 cm^{-1}.

TGA and DSC measurements

Thermogravimetric (TGA) and differential scanning calorimetry (DSC) measurements were performed simultaneously on a STA449 F5 Jupiter ECO from Netzsch. The samples were warmed from 40 °C to 850 °C with heating rate of 10 °C per min under nitrogen flow of 50 $mL.min^{-1}$, the temperature was then stabilized at 850 °C over a period of 4 hours.

X-ray diffraction (XRD) analysis

X-ray diffraction of powdered chitosan samples were examined by a Panalytical X'Pert Pro with an Xcelerator fast detector operating at 45 kV and 30 mA. The radiation was generated from a Cu Kα (k =0,15418nm) source. The diffraction data were collected at 2h values from 5° to 75°.

The crystallinity index of isolated chitosan samples (CrI) were calculated from XRD data using the following equation:[31,32]

$CrI = [(I_{cr}-I_{am})/I_{cr}]*100$

Where I_{cr} is the maximum intensity for crystalline lattices at 2ϑ = 19.6° and I_{am} is the maximum intensity at 2θ = 12.6° corresponding to the amorphous region.

Elemental analysis

Elemental analysis was carried out on an elemental analyzer Flash EA 1112 series (Thermo Finnigan), equipped with Eager Xperience software.

2.5. Hydrogel preparation and characterisation

Hydrogel chitosan/gelatin preparation

- Chitosan solution preparation:

600 mg of chitosan was dissolved in 20 mL of 2% acetic acid aqueous solution (Chitosan final concentration: 3 % w/v) at 40°C using an ultrasonic bath. After complete dissolution, the warm solution was filtered. The solution's pH was then systematically increased to 4.7 using a 0.5M aqueous solution of NaOH.

- Gelatin solution preparation:

3,6 g of gelatin was dissolved in 20 mL of water at 40°C using an ultrasonic bath. After total dissolution, the warm solution was filtered.

- Hydrogel preparation:

10 mL of gelatin solution was mixed with 20 mL of chitosan solution. The mixture pH was increased to 6 by addition of 0.5M aqueous solution of NaOH added drop by drop.

Rheological measurements

Rheological measurements were conducted using MCR502 (Anton Paar) rheometer in parallel plate geometry. The hydrogel was placed between two parallel disks (r=2 cm) separated by a gap of 0.5 mm. A solvent trap was used to prevent solvent evaporation during measurement. Storage (G') and loss (G") moduli were measured in a linear viscoelastic regime as function of temperature imposed on the lower rheometer plate using an integrated Peltier element. The duration of measurements was adjusted so the moduli achieved their steady state value (with an error of ±5%) at each tested temperature. The steady-state flow curves were measured in a shear rate control mode imposing a continuous shear rate ramp from 2 s^{-1} to 100 s^{-1} at the rate of 0.1s^{-1}/s and measuring the resulting shear stress.

2.6. Hydrogel 3D printing assays

3D printing was performed using a Bio-X bioprinter from Cellink (Boston, MA, USA). The printing was performed following an extrusion process. The cartridge was kept at room temperature, while the heated substrate temperature was kept constant at 25 °C. Steel needle (sizes G22) was used to print hydrogels.

Printing parameters: An extrusion pressure of 60 Kpa and translational speed of the printing head (feed rate) 5 mms^{-1} were chosen to ensure proper and continuous filament formation and were kept constant throughout the study.

3. Results and discussion

3.1. Chitin extraction and deacetylation (Chitosan preparation)

As reported in the literature, different pathways can be employed to extract chitin and prepare chitosan, with the most common methods being based on chemical or enzymatic treatment.[23,48] In the present work, we employ a chemical strategy (described in detail in Sec.2.2): with chitin being extracted from dry beetle in three steps: 1- demineralisation (1 M HCl aqueous solution, 95 °C, 2 hours), 2- deproteination (2 M aqueous NaOH solution, 95 °C, 36 hours) and 3- bleaching (50 wt % H_2O_2, RT, 4 hours, followed by acetone rinsing). The obtained solid (chitin) is directly used in deacetylation without further purification. Chitosan is obtained after deacetylation (50/50 w/w NaOH water solution, 95° C, overnight). The final solid is washed with acetone and dried (overall yield, 22.1 %). The final product, chitosan, is a poly (β-(1-4)-D-glucosamine) with random presence of N-acetyl-D-glucosamine (Figure 2). The isolated chitosan can be fully dissolved in slightly acidic water, confirming the removal of acetyl groups.

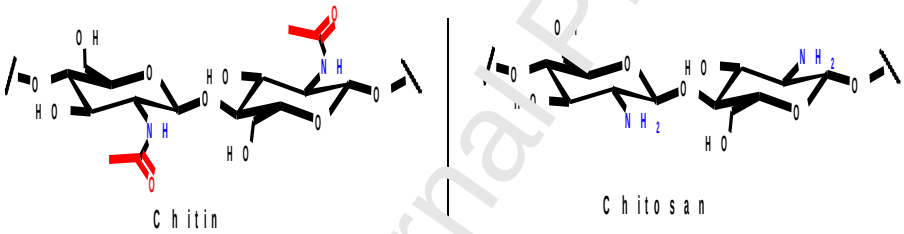

Figure 2. Theoretical chemical structures of chitin and chitosan.

3.2. Chitosan characterisation

To properly characterize the prepared chitosan, FT-IR analysis was conducted. FT-IR observation reveals all the characteristic bands associated with chitosan (Figure 3, Table 1).

Table 1: FT-IR data for chitosan from *Heliocopris dilloni specimen*.

Functional group	Chitosan for Heliocopris Sp.
OH Stretching	3330-3430 cm^{-1}
NH Stretching	3230-3300 cm^{-1}
CH2 Vibration	2930-2850 cm^{-1}
C=O	1640-1665 cm^{-1}
NH (Bending)	1550-1585 cm^{-1}

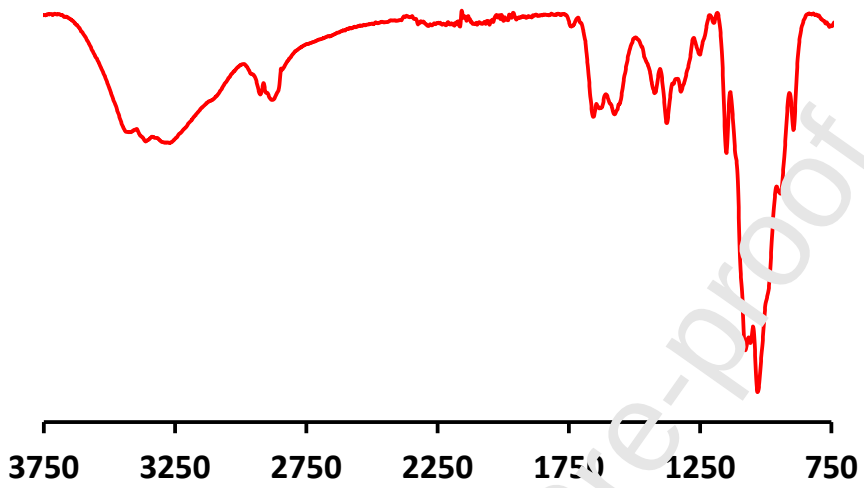

Figure 3. FT-IR spectrum of *Heliocopris sp*. chitosan.

Heliocopris chitosan presents strong bands at 3430-3330 cm^{-1} and 3230-3300 cm^{-1}, which are consistent with the stretching of O-H and N-H bonds, respectively. The band corresponding to sp3 CH_2 vibration is observed at 2850-2930 cm^{-1} and the C=O band from the amide group is weak but can be observed at 1640-1665 cm^{-1}. Lastly, the bending and vibration bands from N-H can be observed at 1550-1585 cm^{-1}. As expected, the observed IR bands for chitosan from *Heliocopris sp*. are consistent with data reported in the literature for shrimp chitosan.[40]

Elemental analysis was also performed on extracted chitosan. The results from this analysis of *Heliocopris dilloni* chitosan are shown in Table 2. The experimental elemental proportions are all consistent with the expected theoretical elemental proportions for chitosan.[40]

Table 2. Elemental analysis for chitosan

Element	Theoretical (%)	Experimental (%)
C	44.32	39.02
H	6.87	6.82
N	7.95	6.99

To complement these characterizations, the deacetylation degree (DD) was also estimated using both ^{1}H-NMR (Figure 4) and titration (Figure 5). Using NMR, the deacetylation degree was determined following a previously reported method.[49] In brief, this method compares signals from acetylated and deacetylated glycosamine units and estimates DD as follows:

DD = [H1-D/(H1-D + 1/3H-Ac)]*100,

where H1-D is the integration of the proton H1 of deacetylated saccharide (H1-D, integrated to 0.92) and H-Ac is the integration of the peak of the three protons of acetyl group (H-Ac, integrated to 1). Following this equation, the DD calculated using NMR for chitosan from *Heliocopris dilloni*. In this study is 73,4 %.

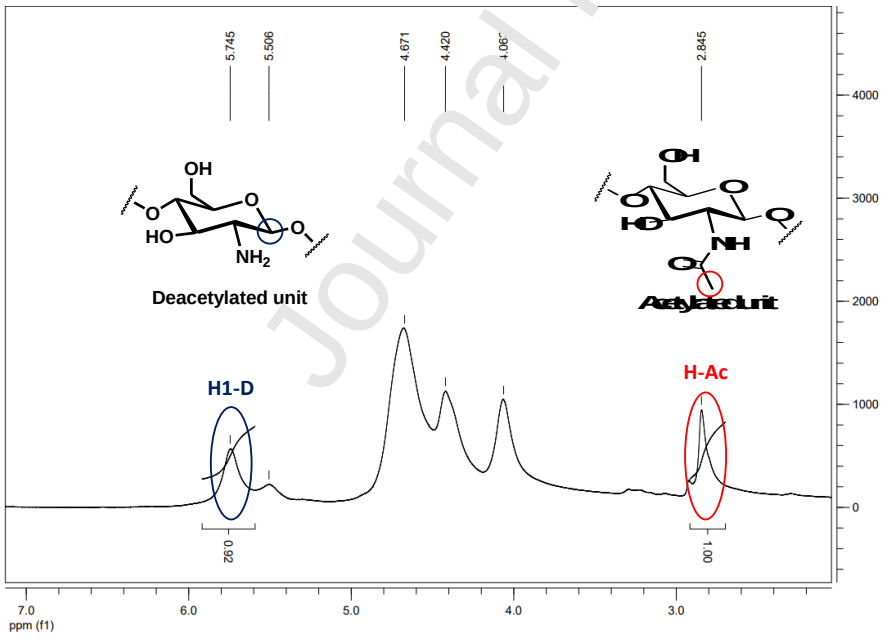

Figure 4. Example of ^{1}H NMR for *Heliocopris dilloni* Chitosan.

DD can also be confirmed using titration, as described by Czechowska-Biskup *et al.*[47] As seen in Figure 5, the chitosan titration curve has two deflections. The first is attributed to excess HCl, and the second is attributed to chitosan hydrochloride formation (Figure 5).

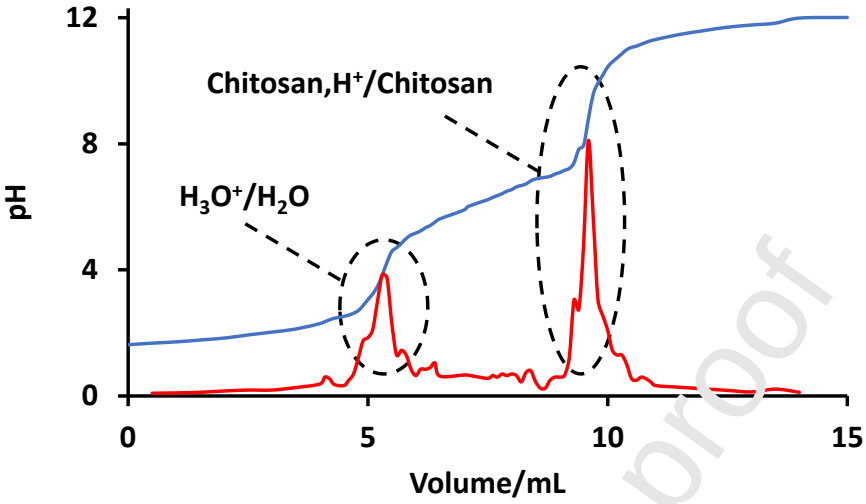

Figure 5. Example of titration curve for *Heliocoprис dilloni* chitosan deacetylation degree determination (Blue: titration curve and red: first derivative of the titration curve).

The difference between these two deflections can be used to calculate DD using the following formula:

Deacetylation degree [%] = $2.03 * \frac{V2-V1}{m+0{,}0042*(V2-V1)}$,

where m is sample mass (g), V_1 and V_2 are volumes of NaOH solution corresponding to the deflection points for HCl and chitosan hydrochloride respectively, 2.03 is a coefficient resulting from the molecular weight of a chitin monomer unit and 0.0042 is a coefficient resulting from the difference between molecular weights of chitin and chitosan monomer units. Using this approach, the DD was determined to be 73.5 ± 2.0 % for the chitosan obtained in this work. Both methods explored here, NMR and titration, yield very similar values for DD and are consistent with data published in the literature for beetles.[32]

Thermal analysis was also performed to characterise the obtained chitosan. Differential scanning calorimetry (DSC) was performed on *Heliocopris sp.* chitosan. The degradation profile of the sample reveals a peak at 302°C (Figure 6).

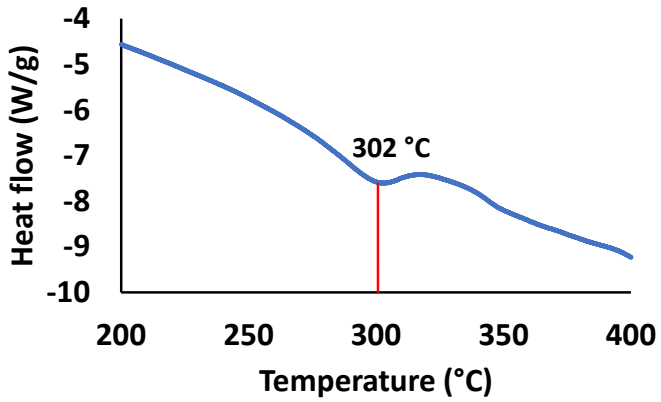

Figure 6. DSC observation for *Heliocopris dilloni* chitosan.

This peak can be attributed to the chitosan degradation as reported in the literature.[5,6] In addition to DSC measurements, thermo-gravimetric analysis (TGA) was carried out. During TGA analysis, the samples were progressively heated to 850 °C with mass loss recorded during the heating. As seen in Figure 7, from 40 °C to 100 °C, the deflection in the mass loss curve reveals the evaporation of water (13 %). Additionally, near 300 °C a significant deflection is observed, which can be attributed to chitosan degradation. At higher temperatures, the organic content completely degrades and only the mineral part of the sample remains. This mineral residue is typically described as ash content of the chitosan. Ash content is an important parameter, as for many applications a low ash level is preferred. For the material obtained here, the ash content is roughly 5 %, and this value is compatible with applications in hydrogel formation (Figure 7).

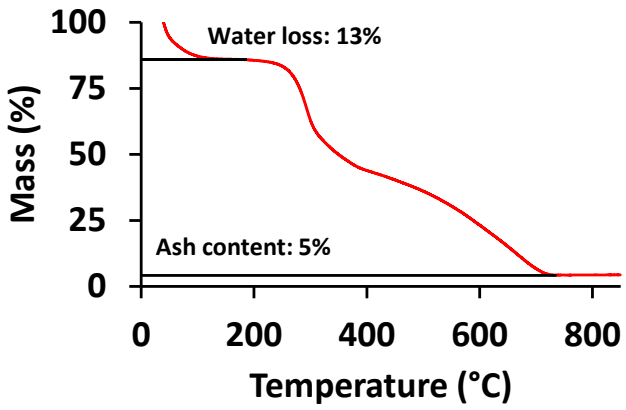

Figure 7. TGA curve for *Heliocopris dilloni* chitosan.

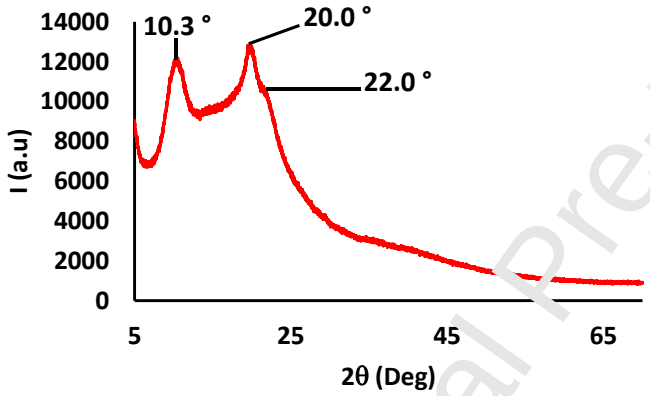

Figure 8. XRD observation for chitosan.

To complete characterisation of the chitosan, XRD studies were conducted on *Heliocopris dilloni* Chitosan (Figure 8). Major, sharp peaks were observed at 10.3° and 20.0°, as well as a shoulder at 22.0°.[31,32] The XRD measurements are consistent with chitosan and allow determination of the crystallinity index (Crl). The CrI was found to be 24.9 % revealing the significant amorphous fraction of the chitosan in the obtained product.

Electron microscopy was performed on *Heliocopris dilloni* surfaces before and after treatment (Figure 9) to observe how the specimen surface evolved during treatment. The raw surface did not show significative structuration, only a few cracks on an otherwise smooth surface are

observed (Figure 9 A). After demineralisation, the surface presents similar morphology without any specific structure. This lack of modification after demineralisation is not surprising and is consistent with our previous work on chitin extraction.[40,41] After deproteination and deacetylation, the surface presents significantly different morphologies (Figures 9 C and D) and revealing slight roughness. Compared with deproteinated and deacetylated surfaces from beetles like *Mecynorhina torquata*, the surfaces in this study from *Heliocopris dilloni* did not reveal any regular network organisation. This observation is not surprising, as this *Heliocopris* genus is not known for structural colour.

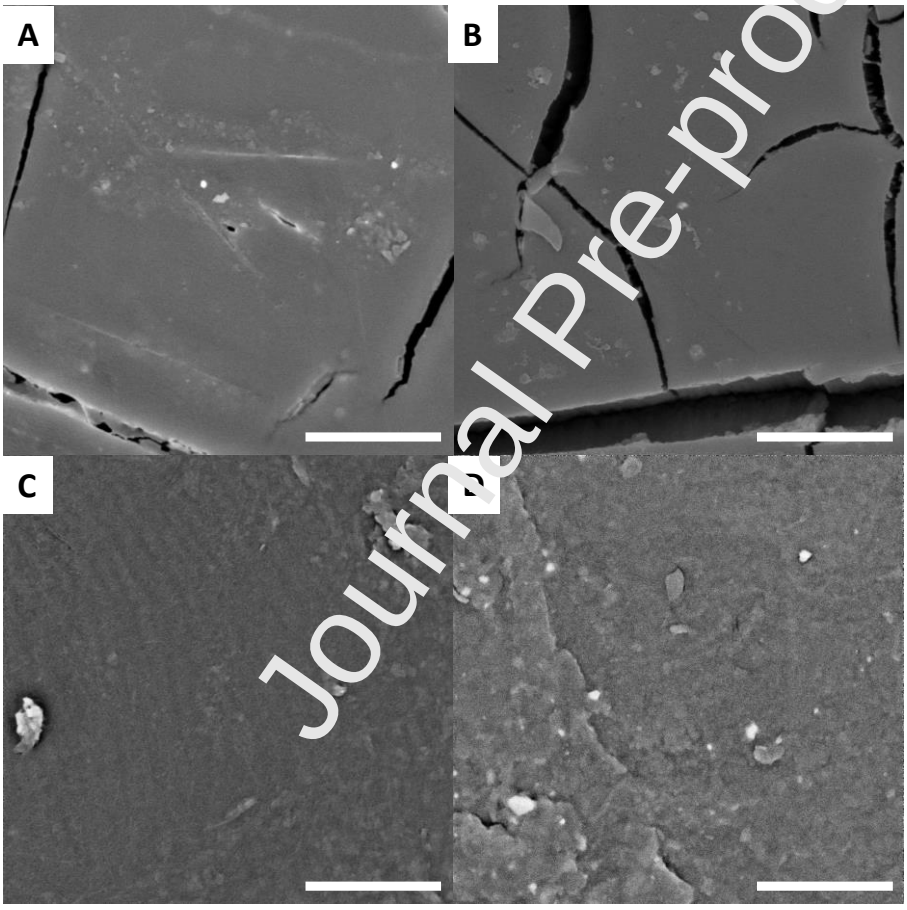

Figure 9. SEM image for *Heliocopris dilloni*. Surfaces (scale bar: 8 µm). A. Raw, B. After demineralization, C. After deproteination and D. *Heliocopris dilloni* Chitosan.

3.3. Hydrogel preparation and characterisation

After extraction from the specimens, the prepared chitosan was used to prepare a hydrogel. Various hydrogels based on chitosan are reported in the literature. In most cases, chitosan is mixed with a secondary polymer to facilitate electrostatic reticulation.[17,50–52] Various polymers, such as alginate or poly vinyl alcohol (PVA) are employed to this end. In our study, we selected a chitosan/gelatin mixture to prepare a biocompatible hydrogel. For the hydrogel preparation, gelatin and chitosan were first dissolved separately and then subsequently mixed, with concentrations of 2% and 6% for chitosan and gelatin, respectively in the final resin.

To be compatible with 3D printing, a hydrogel should be easy to melt and also fluid enough upon melting to flow into the injection chamber.[44] However, it should also remain solid at room temperature to maintain the printed shape after printing. With these parameters in mind, it is important to determine the hydrogel melting point, and also to characterize viscoelastic properties near room temperature. Towards this end, two experiments were performed. First, the storage (G') and loss (G") moduli (reflecting the stored elastic energy and viscous energy dissipation, respectively) were measured as a function of temperature (Figure 10). A sinusoidal strain of constant amplitude (0.05%) and a frequency f=1Hz was applied and the resulting shear stress was measured and the moduli G', G" were determined using standard rheological conversion. Preliminary experiments showed that at the applied strain amplitude of 0.05%, the internal structure of hydrogel remains intact (linear viscoelastic domain).

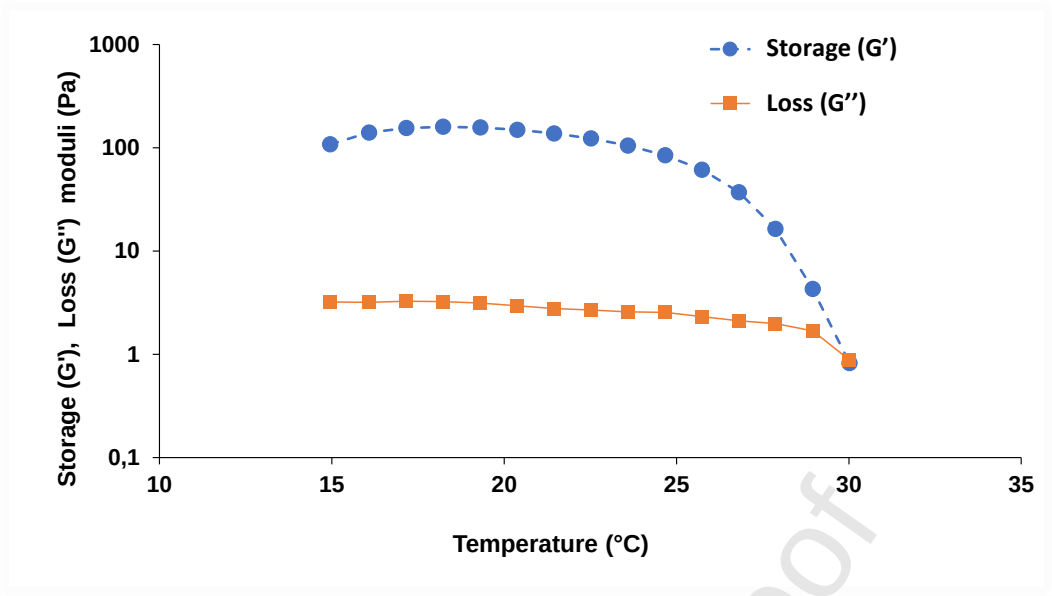

Figure 10. Measurement of storage and loss moduli as function of the temperature.

The measurements presented in Figure 10 show that the storage modulus is roughly 2 orders of magnitude greater than the loss modulus at low temperature (15°C), and then slowly decreases between 24 and 28 °C, revealing the beginning of gel melting. At temperatures above 28 °C, the modulus dramatically decreases indicating that the gel is molten. At the highest temperature tested, 30°C, the storage modulus becomes nearly equivalent to the loss modulus, indicating a solid liquid transition of the gel at this temperature. This observation indicates that the gel should be totally molten at 30 °C but will remain solid at 25 °C. These properties are suitable for 3D printing applications.

The second set of rheological measurements conducted concerned the flow curves (shear stress vs shear rate), obtained at two temperatures near ambient conditions (23 and 25 °C) (Figure 11).

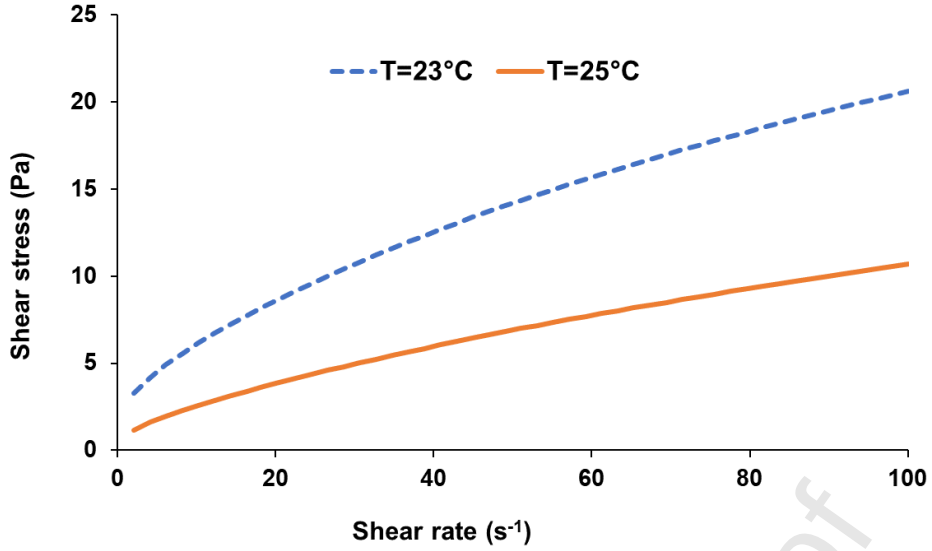

Figure 11. Flow curves for the hydrogel (shear stress vs. shear rate) at two different temperatures.

The measured flow curves were extrapolated to the ordinate axis and the shear stress value at zero shear rate was assigned as a dynamic yield stress. Following this method, the yield stress was 2.5Pa for 23°C and 1Pa for 25°C, confirming the solid gel structure at rest. When flow occurs due to an increase in shear rate, we observe a decrease in the viscosity (as inferred from decreasing slope of the flow curve), indicating shear-thinning behavior of the studied hydrogel. Additionally, Figure 10 reveals that viscosity depends strongly on the temperature. In all ranges of the applied shear rates, the viscosity is roughly two times greater for measurements at 23°C compared to 25°C. All these observations again confirm that the prepared hydrogel is a good candidate to prepare bio-ink for bio-printing.

The prepared hydrogel was also observed with SEM. This imaging was performed on the dried hydrogel (Figure 12). The images reveal a membrane-like structure which is consistent for dry hydrogels.

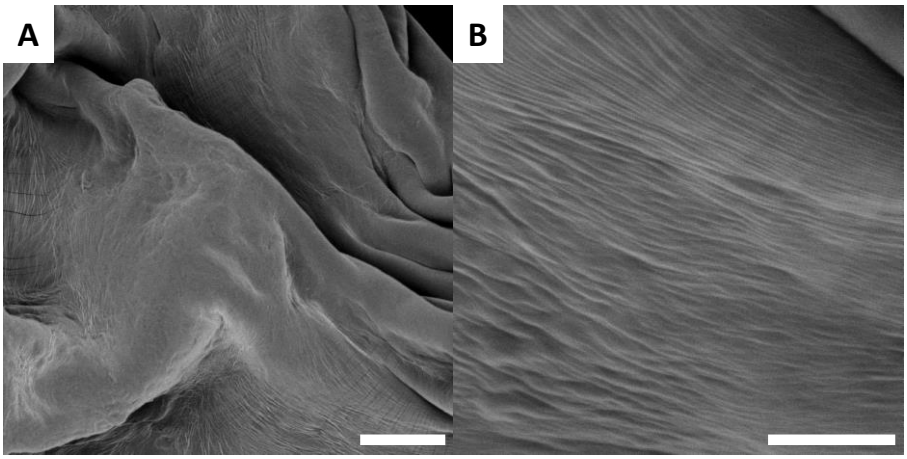

Figure 12. SEM images of the dried hydrogel (Scale bar, A: 10 µm and B: 30 µm).

3.4. Hydrogel 3D printing assays

The prepared hydrogel was then used for 3D printing application (Figure 13).

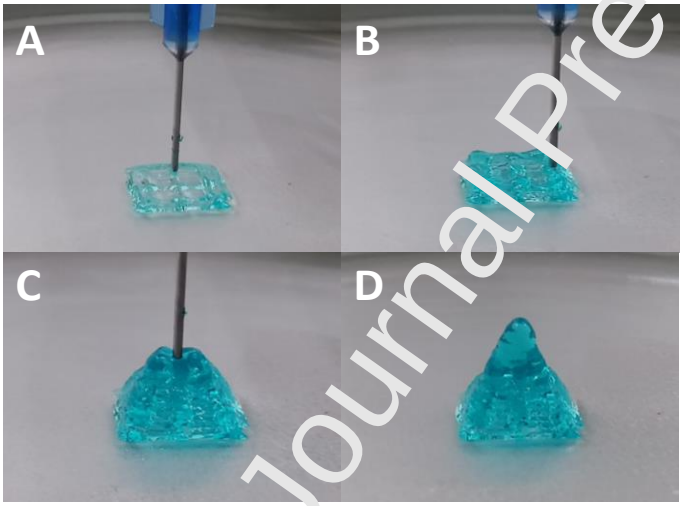

Figure 13. Example of 3D printing.

Various 3D structures including the pyramid structures shown in Figure 13 were successfully printed using the obtained material, including squares, circles and letters. For 3D printing, an important factor is preservation of the printed shape. Indeed, after printing, due to the gravity and the gel fluidity, the risk is that hydrogel will flow and loose the printed shape. To determine the magnitude of this effect, different measurements were performed on each printed structure (Figure 14) to determine the variation in size due to the gel creep.

Figure 14. Evaluation of the printing accuracy. A: Theoretical model, B: Printed shape and C: measurement.

The variations are presented in Table 3 and are calculated as follow:

$$accuracy\ \% = \frac{Experimental\ size}{Theoretical\ size} * 100$$

Table 3. Variation of the printed shape compared with theoretical model.

	Accuracy (%)	
	Length	Width
Square	87.5	87.5
Circle	85	
Letter	96,3	92,5
Pyramid	94,3	96,7

Compared with the proposed structures, all the presented printed structures are very similar with 5 to 15 % variation in size. The formed hydrogels did not flow after printing and the printing shapes are preserved for a few hours at room temperature (Observations in Table 2 were made after two hours). Such shape preservation is expected to be related to the yield stress of the hydrogel at ambient temperature, as revealed by rheological measurements (Figure 11). This observation reveals that the prepared hydrogel is compatible with bioprinting.

Conclusion

In conclusion, we report here for the first time the preparation of chitosan based on *Heliocopris dilloni* and its application in 3D printing. Chitosan was obtained using simple, straight-forward chemical treatments including demineralisation, deproteination, bleaching and deacetylation. After the four-step process, the treated cuticle produced chitosan (22.1 % yield). The formed chitosan was characterised using various techniques including FT-IR, TGA, XRD, elemental analysis and NMR. The deacetylation degree was determined to be 73 % and the ash content was 5%. After characterisation, the extracted chitosan was successfully used to prepare a Chitosan/gelatin hydrogel. After rheological characterisation and SEM observation of the gel, it was used for 3D printing. The gel adapts to the bio-printing technique and various three-dimensional shapes were printed. Measurements on the printed shapes show well defined structures with shape accuracy between 85 and 95 %. All this encouraging preliminary data confirms the possibility to use *Heliocopris dilloni* as source of

chitosan. These results show the strong potential of beetle for chitosan production and hydrogel preparation. Combined with the increase in the insect production in the world to feed animals or humans, this work offers an efficient solution to valorise the industrial by-products of insect production. This research article is a first step for insect waste valorisation and reveals the potential for this strategy to impact materials science and biomedicine. Future work in this area and follow-up studies will evaluate the cytocompatibility of beetle's chitosan hydrogel and the suitability of this material for bioprinting.

Acknowledgments

This work was supported by the French National Research Agency (ANR, Agence Nationale de la Recherche) as future investment project UCA^{JEDI} with reference: n° ANR-15-IDEX-01 (Perception of Insects by Human and RheoGels). TGA, SEM, contact angle measurements and hydrogel 3D printing were performed at technological platform « Smart City Innovation Center » (Université Côte d'Azur-IMREDD). The "Smart City Innovation Center" is a project funded by the European union with the European fund for regional development and co-funded by Metropole Nice Côte d'Azur, the Département Alpes-Maritimes, the Région Sud Provence-Alpes-Côte d'Azur and France for the "initiative d'excellence" (Investissements d'avenir).

References

(1) Khoushab, F.; Yamabhai, M. Chitin Research Revisited. *Mar. Drugs* **2010**, *8* (7), 1988–2012. https://doi.org/10.3390/md8071988.
(2) Sikorski, P.; Hori, R.; Wada, M. Revisit of α-Chitin Crystal Structure Using High Resolution X-Ray Diffraction Data. *Biomacromolecules* **2009**, *10* (5), 1100–1105. https://doi.org/10.1021/bm801251e.
(3) Cuong, H. N.; Minh, N. C.; Van Hoa, N.; Trung, T. S. Preparation and Characterization of High Purity β-Chitin from Squid Pens (Loligo Chenisis). *Int. J. Biol. Macromol.* **2016**, *93*, 442–447. https://doi.org/10.1016/j.ijbiomac.2016.08.085.

(4) Wu, J.; Niu, Y.; Jiao, Y.; Chen, Q. Fungal Chitosan from Agaricus Bisporus (Lange) Sing. Chaidam Increased the Stability and Antioxidant Activity of Liposomes Modified with Biosurfactants and Loading Betulinic Acid. *Int. J. Biol. Macromol.* **2019**, *123*, 291–299. https://doi.org/10.1016/j.ijbiomac.2018.11.062.
(5) Juárez-de la Rosa, B. A.; Quintana, P.; Ardisson, P.-L.; Yáñez-Limón, J. M.; Alvarado-Gil, J. J. Effects of Thermal Treatments on the Structure of Two Black Coral Species Chitinous Exoskeleton. *J. Mater. Sci.* **2012**, *47* (2), 990–998. https://doi.org/10.1007/s10853-011-5878-9.
(6) Kaya, M.; Baran, T.; Mentes, A.; Asaroglu, M.; Sezen, G.; Tozak, K. O. Extraction and Characterization of α-Chitin and Chitosan from Six Different Aquatic Invertebrates. *Food Biophys.* **2014**, *9* (2), 145–157. https://doi.org/10.1007/s11483-013-9327-y.
(7) Jones, M.; Kujundzic, M.; John, S.; Bismarck, A. Crab vs. Mushroom: A Review of Crustacean and Fungal Chitin in Wound Treatment. *Mar. Drugs* **2020**, *18* (1), 64. https://doi.org/10.3390/md18010064.
(8) Sahariah, P.; Másson, M. Antimicrobial Chitosan and Chitosan Derivatives: A Review of the Structure–Activity Relationship. *Biomacromolecules* **2017**, *18* (11), 3846–3868. https://doi.org/10.1021/acs.biomac.7b01058.
(9) Yi, H.; Wu, L.-Q.; Bentley, W. E.; Ghodssi, R.; Rubloff, G. W.; Culver, J. N.; Payne, G. F. Biofabrication with Chitosan. *Biomacromolecules* **2005**, *6* (6), 2881–2894. https://doi.org/10.1021/bm050410l.
(10) Van Vlierberghe, S.; Dubruel, P.; Schacht, E. Biopolymer-Based Hydrogels As Scaffolds for Tissue Engineering Applications: A Review. *Biomacromolecules* **2011**, *12* (5), 1387–1408. https://doi.org/10.1021/bm200083n.
(11) Wang, H.; Qian, J.; Ding, F. Emerging Chitosan-Based Films for Food Packaging Applications. *J. Agric. Food Chem.* **2018**, *66* (2), 395–413. https://doi.org/10.1021/acs.jafc.7b04523.
(12) Shahid-ul-Islam; Shahid, M.; Mohammad, F. Green Chemistry Approaches to Develop Antimicrobial Textiles Based on Sustainable Biopolymers—A Review. *Ind. Eng. Chem. Res.* **2013**, *52* (15), 5245–5260. https://doi.org/10.1021/ie303627x.
(13) Thakur, V. K.; Thakur, M. K. Recent Advances in Graft Copolymerization and Applications of Chitosan: A Review. *ACS Sustain. Chem. Eng.* **2014**, *2* (12), 2637–2652. https://doi.org/10.1021/sc500634p.
(14) Williams, P. A.; Campbell, K. T.; Gharaviram, H.; Madrigal, J. L.; Silva, E. A. Alginate-Chitosan Hydrogels Provide a Sustained Gradient of Sphingosine-1-Phosphate for Therapeutic Angiogenesis. *Ann. Biomed. Eng.* **2017**, *45* (4), 1003–1014. https://doi.org/10.1007/s10439-016-1768-2.
(15) Salehi, M.; Bagher, Z.; Kamrava, S. K.; Ehterami, A.; Alizadeh, R.; Farhadi, M.; Falah, M.; Komeili, A. Alginate/Chitosan Hydrogel Containing Olfactory Ectomesenchymal Stem Cells for Sciatic Nerve Tissue Engineering. *J. Cell. Physiol.* **2019**, *234* (9), 15357–15368. https://doi.org/10.1002/jcp.28183.
(16) Rhoades, J.; Roller, S. Antimicrobial Actions of Degraded and Native Chitosan against Spoilage Organisms in Laboratory Media and Foods. *Appl. Environ. Microbiol.* **2000**, *66* (1), 80–86. https://doi.org/10.1128/AEM.66.1.80-86.2000.
(17) Deng, B.; Shen, L.; Wu, Y.; Shen, Y.; Ding, X.; Lu, S.; Jia, J.; Qian, J.; Ge, J. Delivery of Alginate-Chitosan Hydrogel Promotes Endogenous Repair and Preserves Cardiac Function in Rats with Myocardial Infarction: Alginate-Chitosan Hydrogel in Rats with MI. *J. Biomed. Mater. Res. A* **2015**, *103* (3), 907–918. https://doi.org/10.1002/jbm.a.35232.
(18) Lu, D.; Wang, H.; Wang, X.; Li, Y.; Guo, H.; Sun, S.; Zhao, X.; Yang, Z.; Lei, Z. Biomimetic Chitosan-Graft-Polypeptides for Improved Adhesion in Tissue and Metal. *Carbohydr. Polym.* **2019**, *215*, 20–28. https://doi.org/10.1016/j.carbpol.2019.03.065.

(19) Kim, I.-Y.; Seo, S.-J.; Moon, H.-S.; Yoo, M.-K.; Park, I.-Y.; Kim, B.-C.; Cho, C.-S. Chitosan and Its Derivatives for Tissue Engineering Applications. *Biotechnol. Adv.* **2008**, *26* (1), 1–21. https://doi.org/10.1016/j.biotechadv.2007.07.009.
(20) Ali Khan, Z.; Jamil, S.; Akhtar, A.; Mustehsan Bashir, M.; Yar, M. Chitosan Based Hybrid Materials Used for Wound Healing Applications- A Short Review. *Int. J. Polym. Mater. Polym. Biomater.* **2020**, *69* (7), 419–436. https://doi.org/10.1080/00914037.2019.1575828.
(21) Kim, S.; Cui, Z.-K.; Koo, B.; Zheng, J.; Aghaloo, T.; Lee, M. Chitosan–Lysozyme Conjugates for Enzyme-Triggered Hydrogel Degradation in Tissue Engineering Applications. *ACS Appl. Mater. Interfaces* **2018**, *10* (48), 41138–41145. https://doi.org/10.1021/acsami.8b15591.
(22) Eddya, M.; Tbib, B.; EL-Hami, K. A Comparison of Chitosan Properties after Extraction from Shrimp Shells by Diluted and Concentrated Acids. *Heliyon* **2020**, *6* (2), e03486. https://doi.org/10.1016/j.heliyon.2020.e03486.
(23) Liu, Y.; Xing, R.; Yang, H.; Liu, S.; Qin, Y.; Li, K.; Yu, H.; Li, P. Chitin Extraction from Shrimp (Litopenaeus Vannamei) Shells by Successive Two-Step Fermentation with Lactobacillus Rhamnoides and Bacillus Amyloliquefaciens. *Int. J. Biol. Macromol.* **2020**, *148*, 424–433. https://doi.org/10.1016/j.ijbiomac.2020.01.124.
(24) Yadav, M.; Goswami, P.; Paritosh, K.; Kumar, M.; Pareek, N.; Vivekanand, V. Seafood Waste: A Source for Preparation of Commercially Employable Chitin/Chitosan Materials. *Bioresour. Bioprocess.* **2019**, *6* (1), 8. https://doi.org/10.1186/s40643-019-0243-y.
(25) Lee, Y.; Kim, H.-W.; Brad Kim, Y. H. New Route of Chitosan Extraction from Blue Crabs and Shrimp Shells as Flocculants on Soybean Solutes. *Food Sci. Biotechnol.* **2017**. https://doi.org/10.1007/s10068-017-0270-4.
(26) Tan, Y. N.; Lee, P. P.; Chen, W. N. Microbial Extraction of Chitin from Seafood Waste Using Sugars Derived from Fruit Waste-Stream. *AMB Express* **2020**, *10* (1), 17. https://doi.org/10.1186/s13568-020-0954-7.
(27) Kheirandish, S.; Ghaedi, M.; Dashtian, K.; Heidari, F.; Pourebrahim, F.; Wang, S. Chitosan Extraction from Lobster Shells and Its Grafted with Functionalized MWCNT for Simultaneous Removal of Pb 2+ Ions and Eriochrome Cyanine R Dye after Their Complexation. *Int. J. Biol. Macromol.* **2017**, *102*, 181–191. https://doi.org/10.1016/j.ijbiomac.2017.03.035.
(28) Huis, A. van. *Edible Insects: Future Prospects for Food and Feed Security*; FAO forestry paper; Food and Agriculture Organization of the United Nations: Rome, 2013.
(29) Paulino, A. T.; Simionato, J. I.; Garcia, J. C.; Nozaki, J. Characterization of Chitosan and Chitin Produced from Silkworm Crysalides. *Carbohydr. Polym.* **2006**, *64* (1), 98–103. https://doi.org/10.1016/j.carbpol.2005.10.032.
(30) Kabalak, M.; Aracagök, D.; Torun, M. Extraction, Characterization and Comparison of Chitins from Large Bodied Four Coleoptera and Orthoptera Species. *Int. J. Biol. Macromol.* **2020**, *145*, 402–409. https://doi.org/10.1016/j.ijbiomac.2019.12.194.
(31) Marei, N. H.; El-Samie, E. A.; Salah, T.; Saad, G. R.; Elwahy, A. H. M. Isolation and Characterization of Chitosan from Different Local Insects in Egypt. *Int. J. Biol. Macromol.* **2016**, *82*, 871–877. https://doi.org/10.1016/j.ijbiomac.2015.10.024.
(32) Shin, C.-S.; Kim, D.-Y.; Shin, W.-S. Characterization of Chitosan Extracted from Mealworm Beetle (Tenebrio Molitor, Zophobas Morio) and Rhinoceros Beetle (Allomyrina Dichotoma) and Their Antibacterial Activities. *Int. J. Biol. Macromol.* **2019**, *125*, 72–77. https://doi.org/10.1016/j.ijbiomac.2018.11.242.
(33) Kaya, M.; Erdogan, S.; Mol, A.; Baran, T. Comparison of Chitin Structures Isolated from Seven Orthoptera Species. *Int. J. Biol. Macromol.* **2015**, *72*, 797–805. https://doi.org/10.1016/j.ijbiomac.2014.09.034.

(34) Soon, C. Y.; Tee, Y. B.; Tan, C. H.; Rosnita, A. T.; Khalina, A. Extraction and Physicochemical Characterization of Chitin and Chitosan from Zophobas Morio Larvae in Varying Sodium Hydroxide Concentration. *Int. J. Biol. Macromol.* **2018**, *108*, 135–142. https://doi.org/10.1016/j.ijbiomac.2017.11.138.
(35) Sajomsang, W.; Gonil, P. Preparation and Characterization of α-Chitin from Cicada Sloughs. *Mater. Sci. Eng. C* **2010**, *30* (3), 357–363. https://doi.org/10.1016/j.msec.2009.11.014.
(36) Kaya, M.; Bitim, B.; Mujtaba, M.; Koyuncu, T. Surface Morphology of Chitin Highly Related with the Isolated Body Part of Butterfly (Argynnis Pandora). *Int. J. Biol. Macromol.* **2015**, *81*, 443–449. https://doi.org/10.1016/j.ijbiomac.2015.08.021.
(37) Godeau, G.; Orange, F.; Godeau, R.-P.; Szczepanski, C. R.; Guittard, F.; Darmanin, T. Variations in Surface Structures and Wettability in the Genus *Pachnoda* Burmeister. *Bioinspired Biomim. Nanobiomaterials* **2019**, *8* (3), 181–189. https://doi.org/10.1680/jbibn.18.00017.
(38) Godeau, G.; Godeau, R.-P.; Orange, F.; Szczepanski, C.; Guittard, F.; Darmanin, T. Variation of Goliathus Orientalis (Moser, 1909) Elytra Nanostructurations and Their Impact on Wettability. *Biomimetics* **2018**, *3* (2), 6. https://doi.org/10.3390/biomimetics3020006.
(39) Montreuil, O.; Candet, C.; Bonaccorso, A.; Szczepanski, C. R.; Orange, F.; Godeau, R.-P.; Guittard, F.; Darmanin, T.; Godeau, G. Micro- and Nanoscopic Observations of Sexual Dimorphisms in Mecynorhina Polyphemus Confluens (Kraatz, 1890) (Coleoptera, Cetoniidae, Goliathini) and Consequences for Surface Wettability. *Arthropod Struct. Dev.* **2019**, *49*, 10–18. https://doi.org/10.1016/j.asd.2019.01.007.
(40) Marmier, T.; Szczepanski, C. R.; Candet, C.; Zenerino, A.; Godeau, R.-P.; Godeau, G. Investigation on Mecynorhina Torquata Drury, 1782 (Coleoptera, Cetoniidae, Goliathini) Cuticle: Surface Properties, Chitin and Chitosan Extraction. *Int. J. Biol. Macromol.* **2020**, *164*, 1164–1173. https://doi.org/10.1016/j.ijbiomac.2020.07.155.
(41) Fournier, P.; Szczepanski, C. R.; Godeau, R.-P.; Godeau, G. Chitosan Extraction from Goliathus Orientalis Moser, 1909: Characterization and Comparison with Commercially Available Chitosan. *Biomimetics* **2020**, *5* (2), 15. https://doi.org/10.3390/biomimetics5020015.
(42) Decante, G.; Costa, J. B.; Silva-Correia, J.; Collins, M. N.; Reis, R. L.; Oliveira, J. M. Engineering Bioinks for 3D Bioprinting. *Biofabrication* **2021**, *13* (3), 032001. https://doi.org/10.1088/1758-5090/abec2c.
(43) Matai, I.; Kaur, G.; Seyedsalehi, A.; McClinton, A.; Laurencin, C. T. Progress in 3D Bioprinting Technology for Tissue/Organ Regenerative Engineering. *Biomaterials* **2020**, *226*, 119536. https://doi.org/10.1016/j.biomaterials.2019.119536.
(44) Groll, J.; Burdick, J. A.; Cho, D.-W.; Derby, B.; Gelinsky, M.; Heilshorn, S. C.; Jüngst, T.; Malda, J.; Mironov, V. A.; Nakayama, K.; Ovsianikov, A.; Sun, W.; Takeuchi, S.; Yoo, J. J.; Woodfield, T. B. F. A Definition of Bioinks and Their Distinction from Biomaterial Inks. *Biofabrication* **2018**, *11* (1), 013001. https://doi.org/10.1088/1758-5090/aaec52.
(45) Tonda-Turo, C.; Carmagnola, I.; Chiappone, A.; Feng, Z.; Ciardelli, G.; Hakkarainen, M.; Sangermano, M. Photocurable Chitosan as Bioink for Cellularized Therapies towards Personalized Scaffold Architecture. *Bioprinting* **2020**, *18*, e00082. https://doi.org/10.1016/j.bprint.2020.e00082.
(46) Gill, B. D. Giant Dung Beetles of the Genus Heliocopris (Scarabaeidae). *Coleopt. Bull.* **2009**, *63* (4), 519–521. https://doi.org/10.1649/1219BR.1.
(47) Czechowska-Biskup, R.; Jarosińska, D.; Rokita, B.; Ulański, P.; Rosiak, J. M. Determination of Degree of Deacetylation of Chitosan - Comparision of Methods. **2012**, 5–20.

(48) El Knidri, H.; Belaabed, R.; Addaou, A.; Laajeb, A.; Lahsini, A. Extraction, Chemical Modification and Characterization of Chitin and Chitosan. *Int. J. Biol. Macromol.* **2018**, *120*, 1181–1189. https://doi.org/10.1016/j.ijbiomac.2018.08.139.
(49) Lavertu, M.; Xia, Z.; Serreqi, A. N.; Berrada, M.; Rodrigues, A.; Wang, D.; Buschmann, M. D.; Gupta, A. A Validated 1H NMR Method for the Determination of the Degree of Deacetylation of Chitosan. *J. Pharm. Biomed. Anal.* **2003**, *32* (6), 1149–1158. https://doi.org/10.1016/S0731-7085(03)00155-9.
(50) Suratman, A.; Oktaviani, A. D.; Aprilita, N. H.; Wibowo, A. H. Alginate-Chitosan Hydrogel as Controlled Release of NPK Macronutrient. *IOP Conf. Ser. Mater. Sci. Eng.* **2019**, *578*, 012074. https://doi.org/10.1088/1757-899X/578/1/012074.
(51) Yan, K.; Xu, F.; Li, S.; Li, Y.; Chen, Y.; Wang, D. Ice-Templating of Chitosan/Agarose Porous Composite Hydrogel with Adjustable Water-Sensitive Shape Memory Property and Multi-Staged Degradation Performance. *Colloids Surf. B Biointerfaces* **2020**, *190*, 110907. https://doi.org/10.1016/j.colsurfb.2020.110907.
(52) Kuo, C.-Y.; Chen, C.-H.; Hsiao, C.-Y.; Chen, J.-P. Incorporation of Chitosan in Biomimetic Gelatin/Chondroitin-6-Sulfate/Hyaluronan Cryogel for Cartilage Tissue Engineering. *Carbohydr. Polym.* **2015**, *117*, 722–730 https://doi.org/10.1016/j.carbpol.2014.10.056.

Synopsis

Graphical Abstract

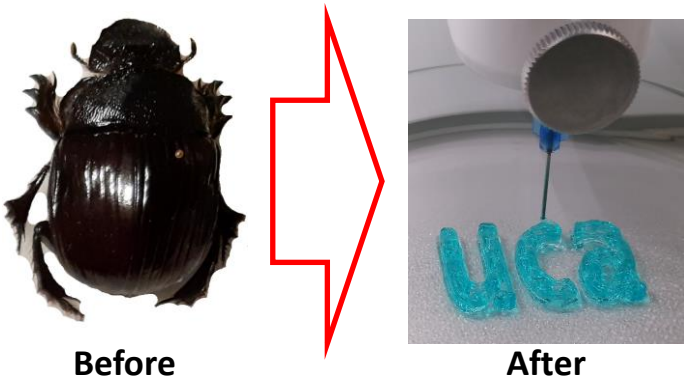

Figure caption:

Figure 1. Examples of *Heliocopris sp.* specimens.

Figure 2. Theoretical chemical structures of chitin and chitosan.

Figure 3. FT-IR spectrum of *Heliocopris sp.* chitosan.

Figure 4. Example of ^{1}H NMR for *Heliocopris dilloni* Chitosan.

Figure 5. Example of titration curve for *Heliocopris dilloni* chitosan deacetylation degree determination (Blue: titration curve and red: first derivative of the titration curve).

Figure 6. DSC observation for *Heliocopris dilloni* chitosan.

Figure 7. TGA curve for *Heliocopris dilloni* chitosan.

Figure 8. XRD observation for chitosan.

Figure 9. SEM image for *Heliocopris dilloni* surfaces (scale bar: 8 µm). A. Raw, B. After demineralization, C. After deproteination and D. *Heliocopris dilloni* Chitosan.

Figure 10. Measurement of storage and loss moduli as function of the temperature.

Figure 11. Flow curves for the hydrogel (shear stress vs shear rate) at two different temperatures.

Figure 12. SEM images of the dried hydrogel (Scale bare, A: 100 µm and B: 30 µm).

Figure 13. Example of 3D printing.

Figure 14. Evaluation of the printing accuracy. A: Theoretical model, B: Printed shape and C: measurement.

Table 1: FT-IR data for chitosan from *Heliocopris dilloni specimen*.

Table 2. Elemental analysis for chitosan

Table 3. Variation of the printed shape compared with theoretical model.

Author statements:

From Dung beetle to hydrogel 3D printing, Investigation on *Heliocopris* Hope, 1838 valorisation for biomedical applications.

Xiaomin Yu Godeau : Investigation, Formal analysis
Freddy Jocelyne Andrianandrasana : Investigation
Olga Volkova : Investigation, Formal analysis
Caroline R. Szczepanski : Writing - Original Draft, Formal analysis
Arnaud Zenerino : Investigation
Olivier Montreuil : Investigation, Formal analysis, Writing - Original Draft
René-Paul Godeau : : Writing - Original Draft, Conceptualization, Formal analysis
Pavel Kuzhir : Investigation, Formal analysis
Guilhem Godeau : Investigation, Conceptualization, Funding acquisition, Writing - Original Draft, Project administration, Resources, Formal analysis.